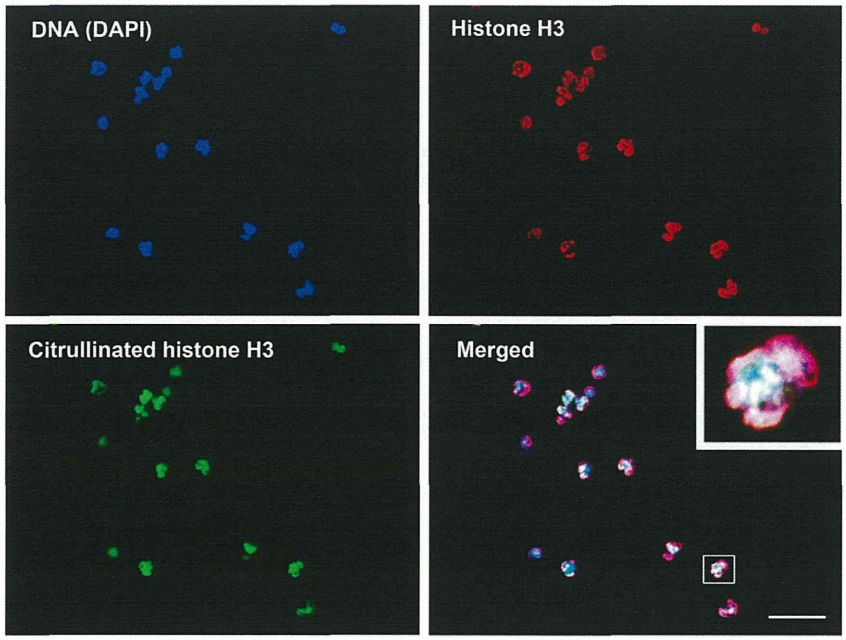

Figure 3. Representative images of immunofluorescence staining to detect citrullinated histone H3 (Cit-H3). Citrullination of histone H3, which is a critical enzymatic process to produce NETs through decondensation of chromatin, was visualized in the blood smear samples using anti-citrullinated histone H3 antibody by immunohistochemistry. Cit-H3 was present in the bloodstream of critically ill patients. The inset in the merged image is the magnified image of a representative cell (white rectangle) expressing citrullinated histone H3 in the nucleus. Neutrophil extracellular traps are not recognized here. In the blood smears surveyed in this study, we identified Cit-H3 in 11 patients (11/49, 22.4%). Blue, 4′,6-diamidino-2-phenylindole (DAPI); red, histone H3; green, citrullinated histone H3 (Magnification ×400). Scale bar; 50 μm.
doi:10.1371/journal.pone.0111755.g003

in response to various microorganisms and pathogens [14]. McDonald et al reported that NETs ensnare circulating bacteria and provide intravascular immunity that protects against bacterial dissemination during septic infection [29]. In this context, the presence of NETs and/or Cit-H3 in infected patients is to be expected. By contrast, trauma or heart disease patients were

Table 3. Comparison between patients positive and negative for neutrophil extracellular traps and/or citrullinated histone H3.

	NET and/or citrullinated histone H3		
	Positive	**Negative**	*p*
Number	15	34	
Age (years)	67.0 (49.0–78.0)	65.5 (56.8–75.3)	.8197
APACHE II score	20.0 (16.0–23.0)	17.5 (11.8–21.3)	.3171
SOFA score	6.0 (5.0–10.0)	5.0 (4.0–8.0)	.4062
Survivors (n)	10 (66.7%)	26 (76.5%)	.4737
SIRS patients (n)	14 (93.3%)	24 (70.6%)	.0786
The presence of bacteria in tracheal aspirate (n)	11 (73.3%)	11 (32.3%)	.0079
WBC count (/μl)	12,430 (8310.0–16510.0)	10,835 (8032.5–14307.5)	.5654
IL-8 (pg/mL)	57.6 (19.9–143.0)	65.3 (23.3–229.5)	.9136
TNF-α (pg/mL)	8.2 (6.2–21.6)	9.0 (4.8–16.3)	.9740
cf-DNA (ng/mL)	1038.3 (744.9–1329.7)	1072.7 (828.6–1770.7)	.6025
Lactate (mg/mL)	39 (11.0–71.0)	17.5 (12.0–56.3)	.5010
HMGB1 (ng/mL)	11.0 (6.8–21.5)	9.7 (5.9–16.3)	.5151

Among the factors evaluated to highlight the relation to the presence of NETs or Cit-H3 in the bloodstream, only "the presence of bacteria in tracheal aspirate" differed significantly between the NET- and/or Cit-H3-positive and -negative groups ($p<.01$). The other factors were not significantly related to the presence of NETs and/or Cit-H3. Continuous variables are presented as the median and IQR unless otherwise noted. The Wilcoxon rank-sum test and Pearson's chi-square test were used to compare two patient groups. NETs: neutrophil extracellular traps, Cit-H3: citrullinated histone H3, IQR: interquartile range, APACHE: Acute Physiological And Chronic Health Evaluation, SOFA: Sequential Organ Failure Assessment, SIRS: systemic inflammatory response syndrome, WBC: white blood cell, IL: interleukin, TNF: tumor necrosis factor, cf-DNA: circulating free DNA, HMGB1: high mobility group box-1.
doi:10.1371/journal.pone.0111755.t003

Table 4. Results of single logistic regression analysis.

Variable	*p*
The presence of bacteria in tracheal aspirate	.0112
SIRS	.1093
cf-DNA	.3003
Lactate	.5476
WBC count	.7862
IL-8	.7875
TNF-α	.8321
HMGB1	.9439

Logistic regression analysis was performed to identify the factors related to the presence of NET and Cit-H3 in the bloodstream. Only "the presence of bacteria in tracheal aspirate" (+) at the time of intubation was a significant factor associated with the presence of NET and Cit-H3 ($p = .0112$). NETs: neutrophil extracellular traps, Cit-H3: citrullinated histone H3, SIRS: systemic inflammatory response syndrome, cf-DNA: circulating free DNA, WBC: white blood cell, IL: interleukin, TNF: tumor necrosis factor, HMGB1: high mobility group box-1.
doi:10.1371/journal.pone.0111755.t004

transported to the hospital immediately after the onset of the condition, and there was no potential risk of infection on admission; this may explain why NETs and Cit-H3 were not detected in these patients.

Intriguingly, a high percentage (62.5%) of patients with CPA exhibited circulating NETs and/or Cit-H3. Acute poisoning, brain stroke, and heat stroke are clinical conditions that can cause disturbance of consciousness, which may induce aspiration. Adnet and Baud demonstrated that the risk of aspiration increases with the degree of unconsciousness (as measured by the Glasgow Coma Scale [GCS]) [32]. In the present study population, the GCS score on admission was significantly lower in the BTA (+) group than in the BTA (−) group (4 [IQR, 3–10.75] vs 13 [IQR, 7–14]; $p<.01$). Except for the infected patient group, the patients who exhibited NETs and/or Cit-H3 in their blood had a significantly lower GCS score on admission ($p = .0418$). We therefore investigated whether "the presence of bacteria in tracheal aspirate", which was represented as part of aspiration and as the presumable preclinical stage of manifested infection, was associated with the presence of NETs and/or Cit-H3, and found a significant association (odds ratio for aspiration, 5.750) (Tables 3–5). Bacteria drawn into the respiratory tract can induce epithelial injury, which provides an opportunity for bacterial translocation as well as leukocyte transmigration until completion of epithelial repair [33,34]. Concomitance of acid aspiration under impaired consciousness additionally enhances bacterial adherence to the epithelium [35]. Injured airway epithelium produces cytokines including IL-8 and alarmins such as HMGB1, both of which are representative inducers for NETs [36–39]. Next, bacteria and inflammatory mediators infiltrating into the interstitial space secondary to epithelial injury will affect the endothelial integrity [40]. The presence of NETs in sputum following aspiration, a phenomenon that we reported previously [24], suggests breakdown of the epithelial barrier that is induced by local inflammation through direct contact between aspirated bacteria and epithelium or through activation of resident immune cells such as macrophages in the respiratory tract [41]. Such epithelial breakdown would allow influx of pathogens, pathogen-associated molecular patterns, cytokines, chemokines, and alarmins from the lumen of the respiratory tract into the circulation. These materials might stimulate the production of NETs intravenously to inhibit systemic invasion of bacteria. We assumed that NETs are induced in the respiratory tract to suppress bacterial dissemination leading to pneumonia and in the vessels to inhibit bacteremia against the invasion of bacteria into the blood and that even such colonization of bacteria in the respiratory tract could trigger citrullination of histone H3 to produce NETs in blood. Single logistic regression analyses of whether infection and/or BTA (+) were associated with the presence of NETs and/or Cit-H3 produced an odds ratio of 7.312 (Table S3). These results suggest that induction of NETs systemically through the citrullination of histone H3 in blood maybe an initial response for protection against bacterial dissemination from latent respiratory infection.

Some researchers consider cf-DNA to be equivalent to NETs in the blood [15,16]. However, our results showed that the occurrence rate of NETs and/or Cit-H3 was not significantly associated with cf-DNA concentration ($p = .6025$) (Table 3). Although the number of patients was different due to sample limitations, additional analysis by MPO-DNA ELISA (Data S1) was also performed. As a result, there was no difference in the values between the group positive for (0.076 [IQR, 0.067–0.100]; $n = 8$) and the group negative for NET and/or citrullinated histone H3 (0.078 [IQR, 0.070–0.111]; $n = 26$). We reported recently that in patients with an acute respiratory infection, NETs became fragmented during recovery from infection [24], suggesting that NETs should also be digested in the blood with time. Our method using blood smear samples cannot detect NETs that harbor inside vessels or that are already degraded, whereas the method based on MPO-DNA ELISA might also measure neutrophil DNA fragments derived from necrosis or apoptosis and cannot detect NETs that are not truncated from the cell body. We consider that at the early phase of critical illness, i.e., when the production of NETs is just starting, the morphological approach has an advantage in being able to detect NETs that are still anchored to the cell body, in conjunction with the merit that identification of citrullination of histone H3 is possible at a stage prior to the release of NETs.

HMGB1 is a nuclear protein present in the nucleus of all nucleated cells. HMGB1 binds to DNA and acts as an inflammatory mediator once it is released extracellularly [42,43]. In this study, HMGB1 was significantly higher in SIRS patients

Table 5. Results of multiple logistic regression analysis of factors associated with the presence of neutrophil extracellular traps and/or citrullinated histone H3.

	Coeff (β)	*p*	OR	Lower	Upper
"the presence of bacteria in tracheal aspirate"	0.875	0.011	5.750	1.583	24.755

Two methods of multiple regression analysis, backward and forward regression, yielded similar models. "The presence of bacteria in tracheal aspirate" was the only factor that was significantly related to the presence of neutrophil extracellular traps and/or citrullinated histone H3 in the bloodstream. The odds ratio for aspiration was 5.750. Coeff (β): coefficient; OR: odds ratio, Lower: lower level of 95% confidence interval, Upper: upper level of 95% confidence interval.
doi:10.1371/journal.pone.0111755.t005

than in non-SIRS patients (Table S2). Unexpectedly, however, HMGB1 was not a significant factor associated with the presence of NETs and/or Cit-H3 (Tables 3–5). NETs contain HMGB1 [44], and one possibility is that HMGB1 binding to NETs is not reflected in the amount of circulating HMGB1 measured by ELISA.

Although IL-8 and TNF-α are considered stimulatory factors that induce NET formation [14,39,45], they were not associated with the presence of NETs and/or Cit-H3 in this study (Tables 3–5). This negative result suggest the presence of an unknown complex regulatory mechanism for the production of NETs in vivo.

As limitations of this study, first, the sample size was small, and the patients were very heterogeneous. Second, we evaluated the presence of NETs and Cit-H3 and the associated factors in the bloodstream of critically ill patients only at admission. It should be investigated in the future how NETs are processed after the induction of NETosis in the circulation. It is presumable that NETs could be degraded by DNase, and the fragments would contribute partially to the formation of cf-DNA. Third, we did not rigorously quantify the amount of NETs and Cit-H3. The possibility of the degradation of NETs and the difficulty in detecting NETs, which are anchored in the vessels, might lead to underestimation of the presence of NETs in our method using blood smear samples. Further study is required to establish finer methods of quantification. We hope that future elucidation of the biological significance of NETs will lead to new strategies to treat critical illness by monitoring NET formation in blood.

Conclusions

The presence of NETs and Cit-H3 were identified immunocytochemically in the bloodstream of a subset of critically ill patients. "The presence of bacteria in tracheal aspirate" may be one important factor related to the presence of circulating NETs. NETs may play a pivotal role in biological defense in the bloodstream of infected and potentially infected patients.

Supporting Information

Figure S1 Representative images of immunostaining of isolated neutrophils that underwent drying and freezing steps before fixation. We tried to evaluate the influence of drying and freezing steps preceding paraformaldehyde fixation on the induction of NETs or citrullination of histone H3 in smear samples. For this, neutrophils separated by density gradient centrifugation from whole blood of a healthy donor were smeared on glass slides, dried, and frozen before fixation. At least through this method, the presence of NETs or citrullinated histone H3 was not identified in immunostaining. Blue, Hoechst 33342; Red, histone H3; Green, citrullinated histone H3 (left panels) or neutrophil elastase (right panels) (Magnification ×400). Scale bar; 50 μm.
(TIF)

Figure S2 Representative images of immunostaining for the negative control study using isotype control antibodies. To ensure accuracy for the immunoreactivity of primary antibodies against blood smear samples, whole mouse and rabbit IgG were used instead of primary antibodies in the immunostaining procedure. This control study resulted in negative signals for histone H3 and citrullinated histone H3. Blue, 4′,6-diamidino-2-phenylindole (DAPI); Red, histone H3; Green, citrullinated histone H3. (Magnification ×200). Scale bar; 50 μm.
(TIF)

Figure S3 Representative images of immunostaining to detect citrullinated histone H3 (left panels) and neutrophil extracellular traps (NETs) (right panels) in the neutrophils from a healthy donor stimulated by phorbol myristate acetate. Neutrophils were isolated by density gradient centrifugation from the whole blood of a healthy donor and stimulated by phorbol myristate acetate. Citrullinated histone H3 and NETs were detected by immunohistochemistry using the same antibodies that were used against the smear samples collected from the critically ill patients. Blue, Hoechst 33342; Red, histone H3; Green, citrullinated histone H3 (left panels) or neutrophil elastase (right panels). (Magnification ×400). Scale bar; 50 μm.
(TIF)

Figure S4 Representative images of immunostaining to detect neutrophil extracellular traps (NETs) in the blood smear from a critically ill patient. The presence of circulating NETs was confirmed by immunohistochemistry using anti-neutrophil elastase antibody. String-like structures extending from the cell body (arrowheads) were composed of DNA and histone, and they contained neutrophil elastase. Blue, 4′,6-diamidino-2-phenylindole (DAPI); Red, histone H1; Green, Neutrophil elastase. (Magnification ×400). Scale bar; 50 μm.
(TIF)

Figure S5 Diff-Quik staining of a blood smear sample from the critically ill patient. Diff-Quik staining confirmed a subpopulation of cells other than neutrophils. (Magnification ×400). Scale bar; 50 μm.
(TIF)

Table S1 Comparison between patients presenting with and without "the presence of bacteria in tracheal aspirate". In patients classified into two groups based on the presence or absence of bacteria in tracheal aspirate, the rate of occurrence of NETs and/or Cit-H3 was significantly higher in "the presence of bacteria in tracheal aspirate" group (11/22, 50.0%) than in "the absence of bacteria in tracheal aspirate" group (4/27, 14.8%) ($p<.01$). Continuous variables are presented as the median and IQR unless otherwise noted. The Wilcoxon rank-sum test and Pearson's chi-square test were used to compare the two patient groups. NETs: neutrophil extracellular traps, Cit-H3: citrullinated histone H3, IQR: interquartile range, APACHE: Acute Physiological And Chronic Health Evaluation, SOFA: Sequential Organ Failure Assessment, SIRS: systemic inflammatory response syndrome, WBC: white blood cell, IL: interleukin, TNF: tumor necrosis factor, cf-DNA: circulating free DNA, HMGB1: high mobility group box-1.
(DOCX)

Table S2 Comparison between patients with and without systemic inflammatory response syndrome. In patients with SIRS on admission, there was a trend toward greater expression of NETs and/or Cit-H3 ($p = .079$). Continuous variables are presented as the median and IQR unless otherwise noted. The Wilcoxon rank-sum test and Pearson's chi-square test were used to compare the two patient groups. NETs: neutrophil extracellular traps, Cit-H3: citrullinated histone H3, IQR: interquartile range, APACHE: Acute Physiological And Chronic Health Evaluation, SOFA: Sequential Organ Failure Assessment, SIRS: systemic inflammatory response syndrome,

WBC: white blood cell, IL: interleukin, TNF: tumor necrosis factor, cf-DNA: circulating free DNA, HMGB1: high mobility group box-1.
(DOCX)

Table S3 Results of single logistic regression analysis of factors associated with the presence of neutrophil extracellular traps and/or citrullinated histone H3 according to the presence of infection and/or "the presence of bacteria in tracheal aspirate". Single logistic regression analyses of whether infection and/or "the presence of bacteria in tracheal aspirate" were associated with the presence of NETs and/or Cit-H3 produced an odds ratio of 7.312. Coeff (β): coefficient, OR: odds ratio, Lower: lower level of 95% confidence interval, Upper: upper level of 95% confidence interval.
(DOCX)

Data S1 MPO-DNA ELISA.
(DOCX)

Author Contributions

Conceived and designed the experiments: TH SH NM TI. Performed the experiments: TH SH NM TI HH NY. Analyzed the data: TH SH NM TI MS OT NY KY YA KO TS KT. Contributed reagents/materials/analysis tools: TH SH HH NY. Wrote the paper: TH SH NM.

References

1. Lekstrom-Himes JA, Gallin JI (2000) Immunodeficiency diseases caused by defects in phagocytes. New Engl J Med 343: 1703–1714.
2. Savchenko AS, Inoue A, Ohashi R, Jiang S, Hasegawa G, et al. (2011) Long pentraxin 3 (PTX3) expression and release by neutrophils in vitro and in ulcerative colitis. Pathol Int 61: 290–297.
3. Vitkov L, Klappacher M, Hannig M, Krautgartner WD (2009) Extracellular neutrophil traps in periodontitis. J Periodontal Res 44: 664–672.
4. Garcia-Romo GS, Caielli S, Vega B, Connolly J, Allantaz F, et al. (2011) Netting neutrophils are major inducers of type I IFN production in pediatric systemic lupus erythematosus. Sci Transl Med 3: 73ra20.
5. Kessenbrock K, Krumbholz M, Schonermarck U, Back W, Gross WL, et al. (2009) Netting neutrophils in autoimmune small-vessel vasculitis. Nat Med 15: 623–625.
6. Brinkmann V, Reichard U, Goosmann C, Fauler B, Uhlemann Y, et al. (2004) Neutrophil extracellular traps kill bacteria. Science 303: 1532–1535.
7. Jaillon S, Peri G, Delneste Y, Fremaux I, Doni A, et al. (2007) The humoral pattern recognition receptor PTX3 is stored in neutrophil granules and localizes in extracellular traps. J Exp Med 204: 793–804.
8. Curran CS, Demick KP, Mansfield JM (2006) Lactoferrin activates macrophages via TLR4-dependent and -independent signaling pathways. Cell Immunol 242: 23–30.
9. Zhang LT, Yao YM, Lu JQ, Yan XJ, Yu Y, et al. (2008) Recombinant bactericidal/permeability-increasing protein inhibits endotoxin-induced high-mobility group box 1 protein gene expression in sepsis. Shock 29: 278–284.
10. Urban CF, Ermert D, Schmid M, Abu-Abed U, Goosmann C, et al. (2009) Neutrophil extracellular traps contain calprotectin, a cytosolic protein complex involved in host defense against Candida albicans. PLoS Pathog 5: e1000639.
11. Cho JH, Fraser IP, Fukase K, Kusumoto S, Fujimoto Y, et al. (2005) Human peptidoglycan recognition protein S is an effector of neutrophil-mediated innate immunity. Blood 106: 2551–2558.
12. Fuchs TA, Abed U, Goosmann C, Hurwitz R, Schulze I, et al. (2007) Novel cell death program leads to neutrophil extracellular traps. J Cell Biol 176: 231–241.
13. Logters T, Margraf S, Altrichter J, Cinatl J, Mitzner S, et al. (2009) The clinical value of neutrophil extracellular traps. Med Microbiol Immunol 198: 211–219.
14. Remijsen Q, Kuijpers TW, Wirawan E, Lippens S, Vandenabeele P, et al. (2011) Dying for a cause: NETosis, mechanisms behind an antimicrobial cell death modality. Cell Death Differ 18: 581–588.
15. Margraf S, Logters T, Reipen J, Altrichter J, Scholz M, et al. (2008) Neutrophil-derived circulating free DNA (cf-DNA/NETs): A potential prognostic marker for posttraumatic development of inflammatory second hit and sepsis. Shock 30: 352–358.
16. Logters T, Paunel-Gorgulu A, Zilkens C, Altrichter J, Scholz M, et al. (2009) Diagnostic accuracy of neutrophil-derived circulating free DNA (cf-DNA/NETs) for septic arthritis. J Orthop Res 27: 1401–1407.
17. Thijssen MA, Swinkels DW, Ruers TJ, de Kok JB (2002) Difference between free circulating plasma and serum DNA in patients with colorectal liver metastases. Anticancer Res 22: 421–425.
18. Sozzi G, Conte D, Leon M, Ciricione R, Roz L, Ratcliffe C, et al. (2003) Quantification of free circulating DNA as a diagnostic marker in lung cancer. J Clin Oncol 21: 3902–3908.
19. Kamat AA, Bischoff FZ, Dang D, Baldwin MF, Han LY, et al. (2006) Circulating cell-free DNA: A novel biomarker for response to therapy in ovarian carcinoma. Cancer Biol Ther 5: 1369–1374.
20. Swarup V, Rajeswari MR (2007) Circulating (cell-free) nucleic acids—a promising, non-invasive tool for early detection of several human diseases. FEBS Lett 581: 795–799.
21. van der Vaart M, Pretorius PJ (2007) The origin of circulating free DNA. Clin Chem 53: 2215.
22. Neeli I, Khan SN, Radic M (2008) Histone deimination as a response to inflammatory stimuli in neutrophils. J Immunol 180: 1895–1902.
23. Wang Y, Li M, Stadler S, Correll S, Li P, et al. (2009) Histone hypercitrullination mediates chromatin decondensation and neutrophil extracellular trap formation. J Cell Biol 184: 205–213.
24. Hirose T, Hamaguchi S, Matsumoto N, Irisawa T, Seki M, et al. (2012) Dynamic changes in the expression of neutrophil extracellular traps in acute respiratory infections. Am J Respir Crit Care Med 185: 1130–1131.
25. Hamaguchi S, Hirose T, Akeda Y, Matsumoto N, Irisawa T, et al. (2013) Identification of neutrophil extracellular traps in blood of patients with systemic inflammatory response syndrome. J Int Med Res 41: 162–168.
26. Bone RC, Balk RA, Cerra FB, Dellinger RP, Fein AM, et al. (1992) Definitions for sepsis and organ failure and guidelines for the use of innovative therapies in sepsis. The ACCP/SCCM Consensus Conference Committee. American College of Chest Physicians/Society of Critical Care Medicine. Chest 101: 1644–1655.
27. Marik PE (2001) Aspiration pneumonitis and aspiration pneumonia. N Engl J Med 344: 665–671.
28. Massberg S, Grahl L, von Bruehl ML, Manukyan D, Pfeiler S, et al. (2010) Reciprocal coupling of coagulation and innate immunity via neutrophil serine proteases. Nat Med 16: 887–896.
29. McDonald B, Urrutia R, Yipp BG, Jenne CN, Kubes P (2012) Intravascular neutrophil extracellular traps capture bacteria from the bloodstream during sepsis. Cell Host Microbe 12: 324–333.
30. Yipp BG, Petri B, Salina D, Jenne CN, Scott BN, et al. (2012) Infection-induced NETosis is a dynamic process involving neutrophil multitasking in vivo. Nat Med 18: 1386–1393.
31. Brinkmann V, Zychlinsky A (2007) Beneficial suicide: Why neutrophils die to make NETs. Nat Rev Microbiol 5: 577–582.
32. Adnet F, Baud F (1996) Relation between Glasgow Coma Scale and aspiration pneumonia. Lancet 348: 123–124.
33. Evans SE, Xu Y, Tuvim MJ, Dickey BF (2010) Inducible innate resistance of lung epithelium to infection. Annu Rev Physiol 72: 413–435.
34. Sousa S, Lecuit M, Cossart P (2005) Microbial strategies to target, cross or disrupt epithelia. Curr Opin Cell Biol 17: 489–498.
35. Mitsushima H, Oishi K, Nagao T, Ichinose A, Senba M, et al. (2002) Acid aspiration induces bacterial pneumonia by enhanced bacterial adherence in mice. Microb Pathog 33: 203–210.
36. Hippenstiel S, Opitz B, Schmeck B, Suttorp N (2006) Lung epithelium as a sentinel and effector system in pneumonia–molecular mechanisms of pathogen recognition and signal transduction. Respir Res 7: 97.
37. Pittet JF, Koh H, Fang X, Iles K, Christiaans S, et al. (2013) HMGB1 accelerates alveolar epithelial repair via an IL-1beta- and alphavbeta6 integrin-dependent activation of TGF-beta1. PLoS One 8: e63907.
38. Tadie JM, Bae HB, Jiang S, Park DW, Bell CP, et al. (2013) HMGB1 promotes neutrophil extracellular trap formation through interactions with Toll-like receptor 4. Am J Physiol Lung Cell Mol Physiol 304: L342–L349.
39. Gupta AK, Hasler P, Holzgreve W, Gebhardt S, Hahn S (2005) Induction of neutrophil extracellular DNA lattices by placental microparticles and IL-8 and their presence in preeclampsia. Hum Immunol 66: 1146–1154.
40. Hiraiwa K, Van Eeden SF (2014) Nature and consequences of the systemic inflammatory response induced by lung inflammation. Lung Inflammation. Available: http://www.intechopen.com/books/lung-inflammation/nature-and-consequences-of-the-systemic-inflammatory-response-induced-by-lung-inflammation. Accessed 2014 Jul 4.
41. Hussell T, Bell TJ (2014) Alveolar macrophages: plasticity in a tissue-specific context. Nat Rev Immunol 14: 81–93.
42. Wang H, Bloom O, Zhang M, Vishnubhakat JM, Ombrellino M, et al. (1999) HMG-1 as a late mediator of endotoxin lethality in mice. Science 285: 248–251.
43. Wang H, Yang H, Tracey KJ (2004) Extracellular role of HMGB1 in inflammation and sepsis. J Intern Med 255: 320–331.
44. Mitroulis I, Kambas K, Chrysanthopoulou A, Skendros P, Apostolidou E, et al. (2011) Neutrophil extracellular trap formation is associated with IL-1beta and autophagy-related signaling in gout. PLoS One 6: e29318.
45. Gupta AK, Joshi MB, Philippova M, Erne P, Hasler P, et al. (2010) Activated endothelial cells induce neutrophil extracellular traps and are susceptible to NETosis-mediated cell death. FEBS Lett 584: 3193–3197.

SCIENTIFIC REPORTS

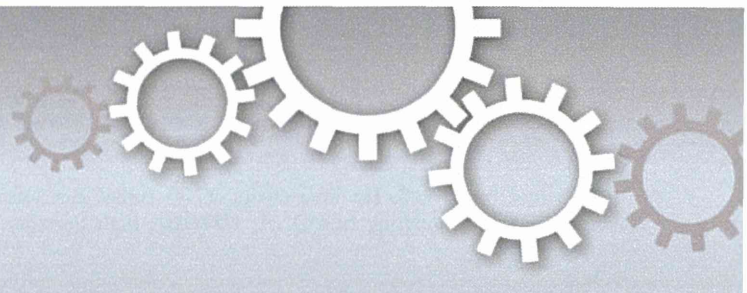

OPEN

SUBJECT AREAS:
TISSUE ENGINEERING
MEDICAL RESEARCH
REGENERATIVE MEDICINE

Received
19 February 2014

Accepted
18 July 2014

Published
13 August 2014

Correspondence and requests for materials should be addressed to T.T. (t-tsuji@rs.noda.tus.ac.jp)

* These authors contributed equally to this work.

† Current address: Department of Oral Rehabilitation and Regenerative Medicine, Graduate School of Medicine, Dentistry and Pharmaceutical Sciences, Okayama University, Okayama, 700-8525, JAPAN.

§ Current address: RIKEN Center for Developmental Biology, Kobe, Hyogo, 650-0047, JAPAN.

Functional tooth restoration by next-generation bio-hybrid implant as a bio-hybrid artificial organ replacement therapy

Masamitsu Oshima[1*†], Kaoru Inoue[2,3*], Kei Nakajima[2,4], Tetsuhiko Tachikawa[5], Hiromichi Yamazaki[2], Tomohide Isobe[5], Ayaka Sugawara[2], Miho Ogawa[1,6], Chie Tanaka[2], Masahiro Saito[2], Shohei Kasugai[7], Teruko Takano-Yamamoto[3], Takashi Inoue[4], Katsunari Tezuka[1,6], Takuo Kuboki[8], Akira Yamaguchi[9] & Takashi Tsuji[1,2,6§]

[1]Research Institute for Science and Technology, Tokyo University of Science, Noda, Chiba, 278-8510, JAPAN, [2]Department of Biological Science and Technology, Graduate School of Industrial Science and Technology, Tokyo University of Science, Noda, Chiba, 278-8510, JAPAN, [3]Division of Orthodontics and Dentofacial Orthopedics, Graduate School of Dentistry, Tohoku University, Sendai, Miyagi, 980-8575, JAPAN, [4]Department of Clinical Pathophysiology, Tokyo Dental College, Chiba-shi, Chiba, 261-8502, JAPAN, [5]Department of Oral Pathology, Showa University School of Dentistry, Shinagawa-ku, Tokyo, 145-8515, JAPAN, [6]Organ Technologies Inc., Tokyo, 108-0074, JAPAN, [7]Section of Oral Implantology and Regenerative Dental Medicine, Graduate School of Tokyo Medical and Dental University, Bunkyo-ku, Tokyo 113-8549, JAPAN, [8]Department of Oral Rehabilitation and Regenerative Medicine, Graduate School of Medicine, Dentistry and Pharmaceutical Sciences, Okayama University, Okayama, 700-8525, JAPAN, [9]Section of Oral Pathology, Department of Oral Restitution, Graduate School of Tokyo Medical and Dental University, Bunkyo-ku, Tokyo 113-8549, JAPAN.

Bio-hybrid artificial organs are an attractive concept to restore organ function through precise biological cooperation with surrounding tissues *in vivo*. However, in bio-hybrid artificial organs, an artificial organ with fibrous connective tissues, including muscles, tendons and ligaments, has not been developed. Here, we have enveloped with embryonic dental follicle tissue around a HA-coated dental implant, and transplanted into the lower first molar region of a murine tooth-loss model. We successfully developed a novel fibrous connected tooth implant using a HA-coated dental implant and dental follicle stem cells as a bio-hybrid organ. This bio-hybrid implant restored physiological functions, including bone remodelling, regeneration of severe bone-defect and responsiveness to noxious stimuli, through regeneration with periodontal tissues, such as periodontal ligament and cementum. Thus, this study represents the potential for a next-generation bio-hybrid implant for tooth loss as a future bio-hybrid artificial organ replacement therapy.

Organ functions are achieved via biological cooperation with surrounding tissues and other organs[1]. Alternative therapies using artificial organs represent an approach to partially support organ function *in vivo*, but they presently are not able to entirely replace organ function[2]. A bio-hybrid artificial organ is an attractive concept to restore organ function through precise biological cooperation with surrounding tissues *in vivo*[2,3]. In the blood circulatory system, physical functions including pumping and filtration have been conventionally substituted using ventricular assist devices and *ex vivo* dialysis systems for heart and kidney failure, respectively[2,4]. In sensory organ dysfunction, bio-hybrid artificial eyes and cochlear implants have aided in the functional restoration of visual impairment and hearing loss, respectively, via afferent neural transmission to the central nervous system (CNS)[5,6]. A bio-hybrid artificial arm that is operated by efferent neural control from the CNS has also been developed as a bio-hybrid organ for irreversible arm loss[7]. In the skeletal system, artificial joints have achieved osseo-integration with bone tissue and have contributed to the support of mechanical loading[8]. Fibrous connective tissues, including muscles, tendons and ligaments, play important roles in exerting biological organ functions, such as tight connectivity, proper flexibility, mobility and resistance against mechanical stimulations[8]. However, in bio-hybrid artificial organs, a fibrous connective artificial organ has not been structurally and functionally established, and further technological improvements are required to achieve fully functional cooperation between an artificial organ and the surrounding tissues[3,8].

Organs, including eyes, joints and teeth, are connected to surrounding tissues via fibrous connective tissues so that they can efficiently perform their biological functions[9]. The periodontal ligament (PDL), which is developed from the dental follicle in tooth germ, is one of the fibrous connective tissues between the tooth-root and the jawbone[10]. The PDL plays essential physiological roles in the absorption of occlusal loading and orthodontic tooth movement accompanied by bone remodelling, and it contributes to the functional cooperation among the teeth, masticatory muscles and temporomandibular joint under the control of the CNS[11,12]. After tooth loss as a result of dental disorders such as caries, periodontal disease or injury, tooth restoration is traditionally performed by replacement with artificial material, such as fixed or removable dentures[13,14]. In addition, an osseo-integrated dental implant that directly connects with the alveolar bone independent of the PDL has been widely applied for the rehabilitation of tooth loss[15,16]. However, current dental implants are not adaptable to patients in the process of jawbone growth and to those patients with severe bone defects[11,16]. It has been therefore expected to develop a fully functional dental implant that satisfies physiological and functional requirements, including bone remodelling, cooperation with the maxillofacial region and sensing of noxious stimulation through connection with a bioengineered PDL as a fibrous connected bio-hybrid organ[17,18].

Regenerative medicine, which developed due to our understanding of embryonic development, stem cell biology and tissue engineering technologies, is an attractive concept to restore organ function[19–21]. Stem cell transplantation therapies have been developed to restore the partial loss of organ functions by replacing hematopoietic stem cells in leukaemia[22] and neural stem cells in spinal injury[23]. Bioengineered two-dimensional tissues have also been used to efficiently repair diseases such as severe burn, corneal injury and myocardial infarction[24,25]. Recently, advances in 3D stem cell manipulation and culturing have been used to understand cell differentiation, cell assembly and multicellular tissue organisation, providing capabilities beyond those of 2D cell cultures[19,26]. It is expected to further develop medical innovations using stem cells that can regenerate for severe disorders such as extensive tissue injury or organ dysfunction[19,26]. To develop a novel bio-hybrid artificial organ that can perform all of the biological organ functions *in vivo*, regenerative medicine technologies using stem cells and culture could improve the functions of several artificial organs[27,28].

In this study, we developed a novel fibrous connected tooth implant using a dental implant and dental follicle stem cells as a bio-hybrid organ. The bio-hybrid implant restored physiological functions, including bone remodelling, regeneration of critical bone-defect and responsiveness to noxious stimulations, through regeneration with periodontal tissues, such as cementum, PDL and alveolar bone. Thus, this study highlights the potential of a next-generation bio-hybrid implant for treating tooth loss as a future bio-hybrid artificial organ replacement therapy.

Results

Periodontal tissue formation on an artificial material using dental follicle tissue. To identify cell sources to regenerate periodontal tissue on an artificial material, a particle of hydroxyapatite (HA), we first investigated whether dental tissues isolated from several tooth developmental stages have the potential to form correct periodontal tissues, including cementum, PDL and alveolar bone, on the HA particle in a subrenal capsule *in vivo* (Supplementary Fig. 1a, b and Fig. 1a). The transplantation of a dental mesenchymal tissue isolated from the tooth germ at embryonic day (ED) 14.5 formed bone around the HA particle. Incomplete periodontal tissues with bone and PDL-like fibres, but not cementum, formed around the HA particle after transplantation with dental follicle tissues isolated from tooth germ at postnatal day (PD) 7 and PDL isolated from a mature tooth at PD35 (Supplementary Fig. 1c). Only dental follicle tissue at ED18.5 was able to form the entirely correct periodontal tissue, including cementum, PDL and alveolar bone, on the HA surface. We further analysed the gene expression patterns associated with periodontal tissue during the each developmental stage (Supplementary Fig. 2a). A multi-layered gene expression profile, including *F-spondin*, *Periostin* and *Osteocalcin*, which are the markers for cementoblasts, PDL cells and osteoblasts[29], respectively, was observed in the inner, middle and outer layers, respectively, of dental follicle tissue at ED18.5; the only stage that was able to generate the correct periodontal structure compared with dental tissues from other developmental stages[30] (Fig. 1b, c and Supplementary Fig. 2a, b). These results indicated that ED18.5 tooth germ-derived dental follicle tissue (ED18.5-DF) is a suitable cell source to generate periodontal tissues, including cementum, PDL and alveolar bone.

Transplantation of a bio-hybrid implant into a tooth loss region. We next investigated whether a dental titanium implant in combination with ED18.5-DF could serve as a bio-hybrid implant with periodontal tissue after engraftment in a tooth loss-region in the adult mouse oral environment (Fig. 1a). To adhere the ED18.5-DF to the implant and promote cementum formation, HA sputter deposition was performed to impart biocompatibility and osteoinductivity[31] and to form a rough structure on the titanium implant surface[32] (Fig. 1d). The implant was enveloped with ED18.5-DF in the correct orientation of the multi-layered DF (Fig. 1e) and transplanted into the lower first molar region of a murine tooth-loss model[33] (Supplementary Fig. 3a, b). Micro-CT and histochemical analyses revealed alveolar bone formation around the implant, referred to osseo-integration, at 30 days after transplantation of the HA-coated implant alone (Fig. 1f, g). In contrast, in the engrafted implant with ED18.5-DF (bio-hybrid implant), the periodontal ligament space and correct periodontal tissue structure consisting of cementum, PDL and alveolar bone were observed on the HA-coated implant (Fig. 1f, g). The PDL fibre structure of the engrafted bio-hybrid implant, which was comprised of transverse collagen fibres and longitudinal elastin fibres, was equivalent to a natural molar tooth (Fig. 1g and Supplementary Fig. 4a, b). The width of the formed PDL around the bio-hybrid implant was clearly detected and comparable to that of a natural tooth (Fig. 1h). After transplantation of bio-hybrid implant with green fluorescence protein (GFP)-transgenic mouse-derived ED18.5-DF, green fluorescence was clearly detectable around the implant at 30 days after transplantation (Fig. 1i and Supplementary Fig. 4c). These results indicate that the HA-coated implant with ED18.5-DF was able to generate periodontal tissues and could be a bio-hybrid implant as a fibrous connective artificial organ.

Structural analysis of the periodontal tissue in the bio-hybrid implant. Periodontal tissue plays important roles in cooperating with the maxillofacial region through the connection with fibre structures in the PDL[11,12]. Thus, we used electro mapping to analyse the ultrastructure of the periodontal ligament on the implant with ED18.5-DF and bone matrices. Although the osseo-integrated implant directly connected to the surrounding alveolar bone, the engrafted bio-hybrid implant showed that the PDL fibre was connected to the implant surface by scanning electron microscopy (SEM) analysis (Fig. 2a). Transmission electron microscopy (TEM) analysis revealed the correct cementum formation on the surface of the bio-hybrid implant and an invasion of Sharpey's fibre into the cementum of the bio-hybrid implant (Fig. 2b, c). Electron probe micro analysis revealed that in the region of the periodontal tissues of both a natural tooth and a bio-hybrid implant, specific elements of hard tissue, such as calcium (Ca; red) and phosphorus (P; green), were detected at high concentrations in the region of cementum and alveolar bone, but not in the PDL region (EPMA; Fig. 2d, e and Supplementary Fig. 5). These results

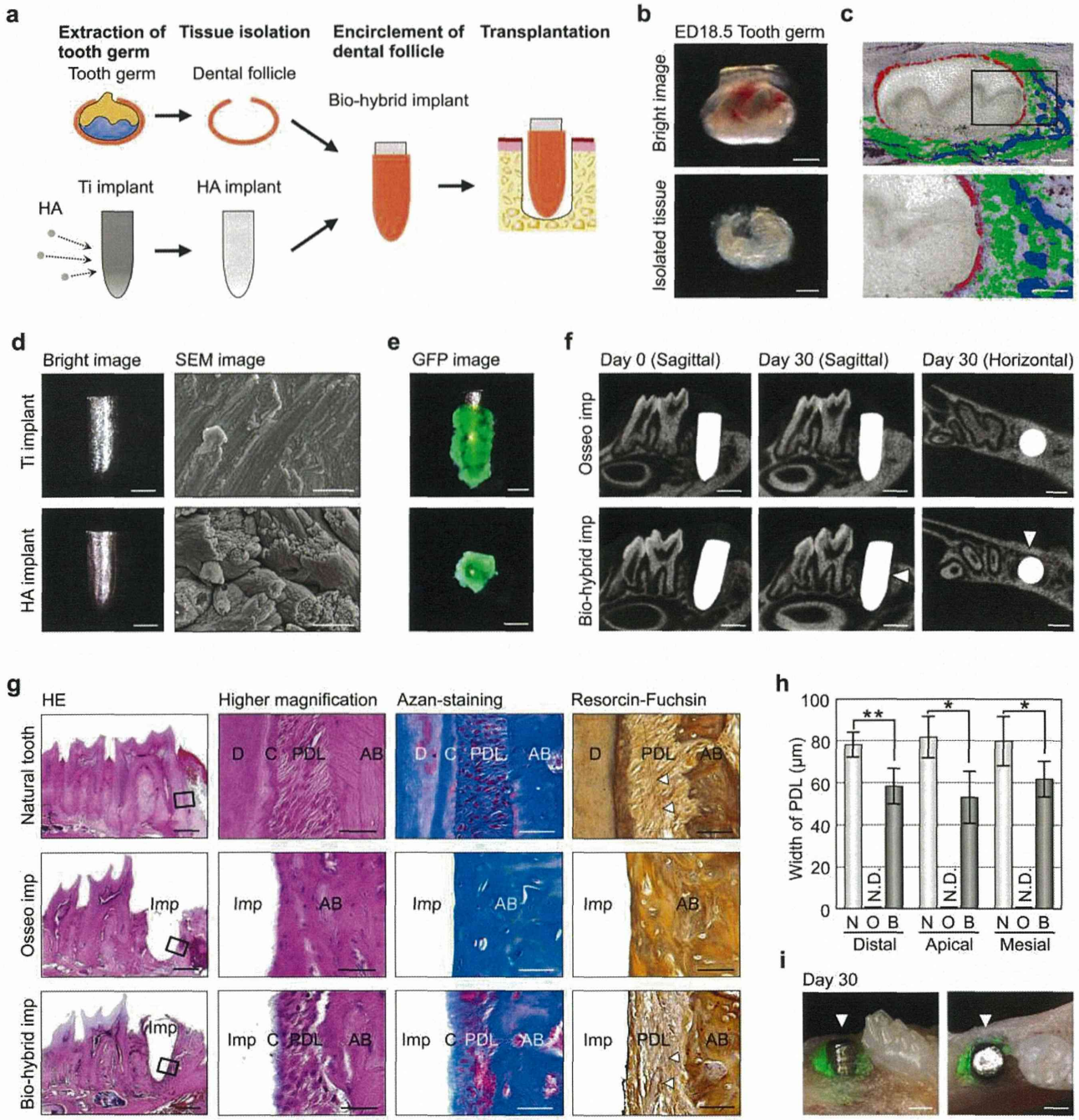

Figure 1 | Engraftment of a bio-hybrid implant in a tooth loss model. (a) Schematic representation of the generative technology of bio-hybrid implant. (Drawings by C.T.). (b) Photographs of ED18.5 tooth germ (*upper*) and isolated dental follicle tissue (*lower*). Scale bar, 100 μm. (c) Layer arrangement indicated by *in situ* hybridisation analysis for the expression patterns of *F-spondin* (red), *Periostin* (green) and *Osteocalcin* (blue) in ED18.5 dental follicle tissue. Scale bar, 100 μm. (d) Photographs (*left*) and surface analysis (*right*) of titanium implant and HA implant using SEM. Scale bar, 500 μm and 1.0 μm in the photographs and SEM images, respectively. (e) Merged images of a bio-hybrid dental implant using ED18.5 dental follicles isolated from GFP transgenic mice (*upper*, sagittal view; *lower*, horizontal view). Scale bar, 500 μm. (f) Micro-CT images of an osseo-integrated implant and a bio-hybrid implant to in sagittal section (*left, centre*) and horizontal section (*right*) at transplantation period of Day 0 and Day 30. Bio-hybrid implant images were observed in the periodontal ligament space (arrowhead). Scale bar, 500 μm. (g) Histological analysis of a natural tooth (*upper*), an engrafted osseo-integrated implant (*middle*) and an engrafted bio-hybrid implant (*lower*) at 30 days post-transplantation was performed. HE, Azan, and Resorcin-Fuschin staining are shown. Scale bar, 500 μm in the lower magnification (*left column*) and 50 μm in the higher magnification (*centre-left, centre-right and right column*). D, dentin; C, cementum; AB, alveolar bone; PDL, periodontal ligament; Imp, implant. (h) Measurement of the width of periodontal ligament area. The periodontal ligament was not detected in osseo-integrated implants at 30 days post-transplantation. N, natural tooth; O, osseo-integrated implant; B, bio-hybrid implant; N.D., Not detected. Error bars represent the standard deviation ($n = 5$). $^{*}p < 0.05$, $^{**}p < 0.01$ (Mann-Whitney U-test). (i) Photograph of a bio-hybrid implant using ED18.5 dental follicles isolated from GFP transgenic mice at 30 days post-transplantation. Arrowhead, bio-hybrid implant. Scale bar, 500 μm.

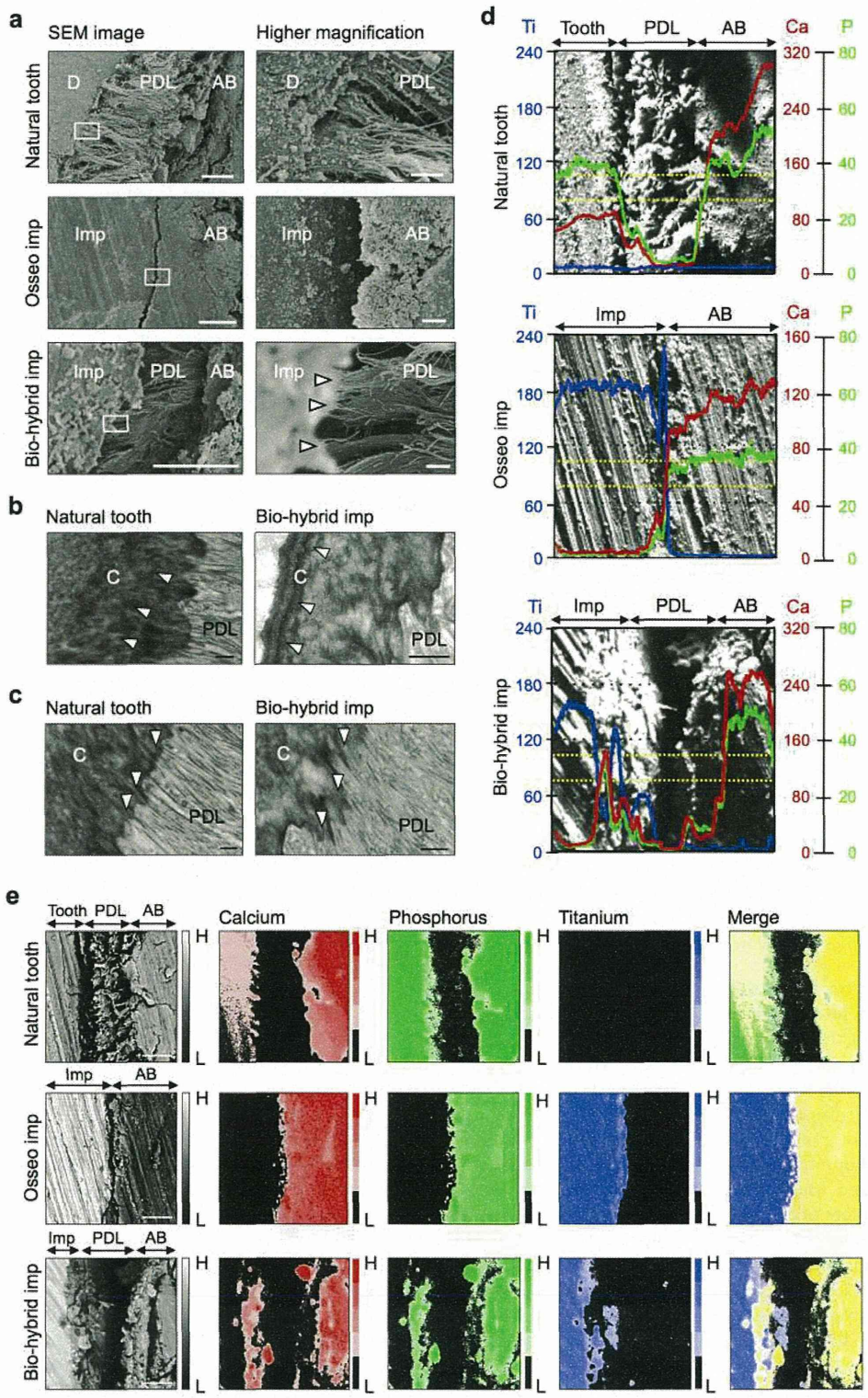

Figure 2 | Structural analyses of a periodontal tissue in the bio-hybrid implant. (a) Scanning electron microscopic (SEM) images of natural tooth (*upper*), the engrafted osseo-integrated implant (*middle*) and the engrafted bio-hybrid implant (*lower*) at 30 days post transplantation was performed. Scale bar, 20 μm and 1.0 μm in the lower and higher magnification, respectively. D, dentin; AB, alveolar bone; PDL, periodontal ligament; Imp, implant. (b and c) Transmission electron microscopic (TEM) observation of a natural tooth (*left*) and the engrafted bio-hybrid implant (*right*). Formation of lamellar cementum (b, arrowhead) and invasion of Sharpey's fibres into the cementum (c, arrowhead). Scale bar, 500 nm. C, cementum; PDL, periodontal ligament. (d) Amounts of calcium (Ca, red), phosphorus (P, green), and titanium (Ti, blue) in a natural tooth (*top*), the engrafted osseo-integrated implant (*middle*) and the engrafted bio-hybrid implant (*bottom*), as determined by SEM. The amounts of elements were measured in the area between dotted lines. AB, alveolar bone; PDL, periodontal ligament; Imp, implant. (e) Elemental mapping superposition of the natural tooth (*top*), osseo-integrated implant (*middle*) and bio-hybrid implant (*bottom*). Calcium (Ca, red), phosphorus (P, green), titanium (Ti, blue) and merged images are shown. AB, alveolar bone; PDL, periodontal ligament; Imp, implant.

demonstrated that the engrafted bio-hybrid implant formed the correct periodontal tissue architecture on the implant surface and the proper fibrous structural connections were formed.

Functional analysis of the periodontal ligament and nerve fibres of the bio-hybrid implant. It has been postulated that a fibrous connective artificial implant functioning as a bio-hybrid organ could be achieved by fulfilling critical functions in the oral environment, such as the cooperation of the bio-hybrid implant with the oral and maxillofacial regions through the PDL[34]. Therefore, we investigated whether an engrafted bio-hybrid implant could restore physiological periodontal functions, specifically the response to mechanical stress and the ability to perceive noxious stimulations *in vivo*. When we analysed the orthodontic movement using a mechanical force in an experimental tooth movement model, the bio-hybrid implant moved in a similar manner to natural teeth in response to orthodontic force (Fig. 3a, b). During experimental tooth movement, colony-stimulating factor-1 (*Csf-1*) mRNA-positive cells, which were used as a marker of osteoclastogenesis, and osteocalcin (*Ocn*) mRNA-positive osteoblasts were observed on the compression and tension sides, respectively[33,35,36] (Fig. 3c). These results demonstrate that the PDL of the bio-hybrid implant successfully mediates bone remodelling via the proper localisation of osteoclasts and osteoblasts in response to mechanical stress and that the implant represents a fibrous connective bio-hybrid implant.

The ability to perceive noxious stimulation, including mechanical stress and pain, are important for proper tooth function[34]. Trigeminal ganglional neurons, which innervate the pulp and PDL, can respond to these stimuli and transduce signals to the CNS. Anti-neurofilament (NF)-immunoreactive nerve fibres were detected in the PDL of the engrafted bio-hybrid implant (Fig. 3d). C-Fos immunoreactive neurons, which are detectable in the superficial layers of the medullary dorsal horn following noxious mechanical and chemical stimulation of the intraoral receptive fields, were dramatically increased in both the natural tooth and the bio-hybrid implant at 2 hours after orthodontic treatment (Fig. 3e). These results indicate that the engrafted bio-hybrid implant restored the ability to perceive noxious stimulation in cooperation with the maxillofacial region.

Regeneration of a vertical bone defect by transplantation of a bio-hybrid implant. The PDL plays an important role in maintaining the height and volume of the surrounding alveolar bone. Thus, tooth root fracture and periodontal disease are known to cause significant alveolar bone resorption[37]. Alveolar bone resorption resulting from dental diseases, which is often the most drastic in the buccal alveolar bone, makes it difficult to insert conventional dental implants without using bone regenerative approaches[38,39]. Finally, we investigated whether transplantation of the bio-hybrid implant could regenerate not only the functional periodontal tissue but also the surrounding alveolar bone of the recipient. To analyse alveolar bone regeneration after implantation, we developed a critical size bone defect model (3-wall bone defect model) that could not heal spontaneously in the murine lower jaw. The defects were prepared by extracting the lower first molar and then removing the buccal alveolar bone in the lower first molar region (Fig. 4a, b and Supplementary Fig. 6a). When the bio-hybrid implant was transplanted into this bone defect, vertical bone formation was observed from the marginal bone of the recipient at 14 days after transplantation, and the bone recovered almost completely with periodontal ligament space at 50 days after transplantation (Fig. 4c and Supplementary Fig. 6b). The regenerative bone area after transplantation of the bio-hybrid implant (Bio) significantly increased compared with a no transplant control (bone defect; BD) and a transplantation of osseo-integrated implant (OS) (BD; 57.9 ± 6.5%, OS; 45.5 ± 16.0%, Bio; 85.5 ± 10.7%, respectively; Fig. 4d, e). Clinically, the failure of dental implant therapy, including the loss or vertical subsidence of the implant after treatment, causes fundamental problems related to survival rates and subsequent dental treatment[40]. After transplantation of an osseo-integrated implant into the normal tooth loss region (OS), the subsidence of the implant was not observed between 0 and 50 days post-implantation (median: −0.04 mm, min: 0.00 mm, max: −0.05 mm). However, transplantation of the osseo-integrated implant into the 3-wall bone defect model (OS in BD) resulted in the dramatic subsidence of the implant (median: −0.69 mm, min: −0.25 mm, max: −0.75 mm; Fig. 4f, g). In contrast, after transplantation of the bio-hybrid implant into this bone defect model (Bio in BD), the subsidence of the implant was significantly prevented (median: −0.08 mm, min: 0.00 mm, max: −0.18 mm) compared with the osseo-integrated implants (Fig. 4f, g). These findings indicate that the PDL on the bio-hybrid implant regenerated the critical size bone defect and that the surrounding bone recognised the bio-hybrid implant as an artificial tooth that was equivalent to a natural tooth. Therefore, these results indicate that the bio-hybrid implant is a fibrous connective bio-hybrid organ that is fully functional *in vivo*.

Discussion

Here, we demonstrate the successful development of a bio-hybrid implant by using dental follicle stem cells to generate an artificial bio-hybrid organ with fibrous connective tissue (Fig. 5). This bio-hybrid implant restored physiological tooth functions, such as the ability to respond to mechanical stress and the ability to perceive noxious mechanical stimulation. The periodontal ligament present on the bio-hybrid implant also induced vertical bone recovery in a 3-wall bone defect model. This study demonstrates the potential for a next generation bio-hybrid implant for treating tooth loss.

Organs maintain the proper position and functionality *in vivo* through their connections to surrounding tissues via fibrous connective-tissues, including tendons, ligaments and muscles[9]. These fibrous connections contribute to biological mobility, such as eye and limb movements, and alleviate mechanical load by acting as shock absorbers[9]. The PDL, which is the connective fibre bundle penetrating into the cementum and alveolar bone[10], contributes to biological tooth functions, including the reduction of excessive occlusal loading and tooth movement, through bone remodelling[11,12]. Many dental implantology studies of tooth loss have attempted to restore periodontal tissue structure, *e.g.*, material-based approaches that were incorporated into the subsidence mechanism as a shock absorber[41], biochemical approaches coated by the PDL formation inducible peptide[42,43] and tissue engineering approaches using the periodontal ligament stem cells[17,18]. However, these technologies could not substitute and restore periodontal tissue functions[17,18]. In this study, the bio-hybrid implant connected to the surrounding alveolar bone through the periodontal tissues including the periodontal ligament with collagen fibre and cementum, but not osseo-integration, on the artificial dental implant surface. The bio-hybrid implant was responsive to mechanical stress through periodontal functions, including bone remodelling. These findings represent a significant advancement for the therapeutic concept of bio-hybrid artificial organs, as the biological fibrous connection achieved fully functional coalition of the artificial organ and living tissue.

The application of artificial organs for the substitution of dysfunctional organs, such as artificial eyes, cochlear implants and artificial arms, has been limited to a condition of peripheral nerves, muscles and bone, which can be sufficient to achieve biological activity at the dysfunctional site[5,6]. To regenerate damaged tissues around the transplantation site of artificial organ, bio-hybrid artificial organ therapy combined with tissue-derived stem cells and multipotent stem cells, including embryonic stem cells and induced pluripotent stem cells, in required[28]. Tooth loss due to root fracture or periodontal disease causes a large amount of alveolar bone resorption in the vertical and horizontal dimensions, and conventional dental therapies, including dental implant and autologous tooth trans-

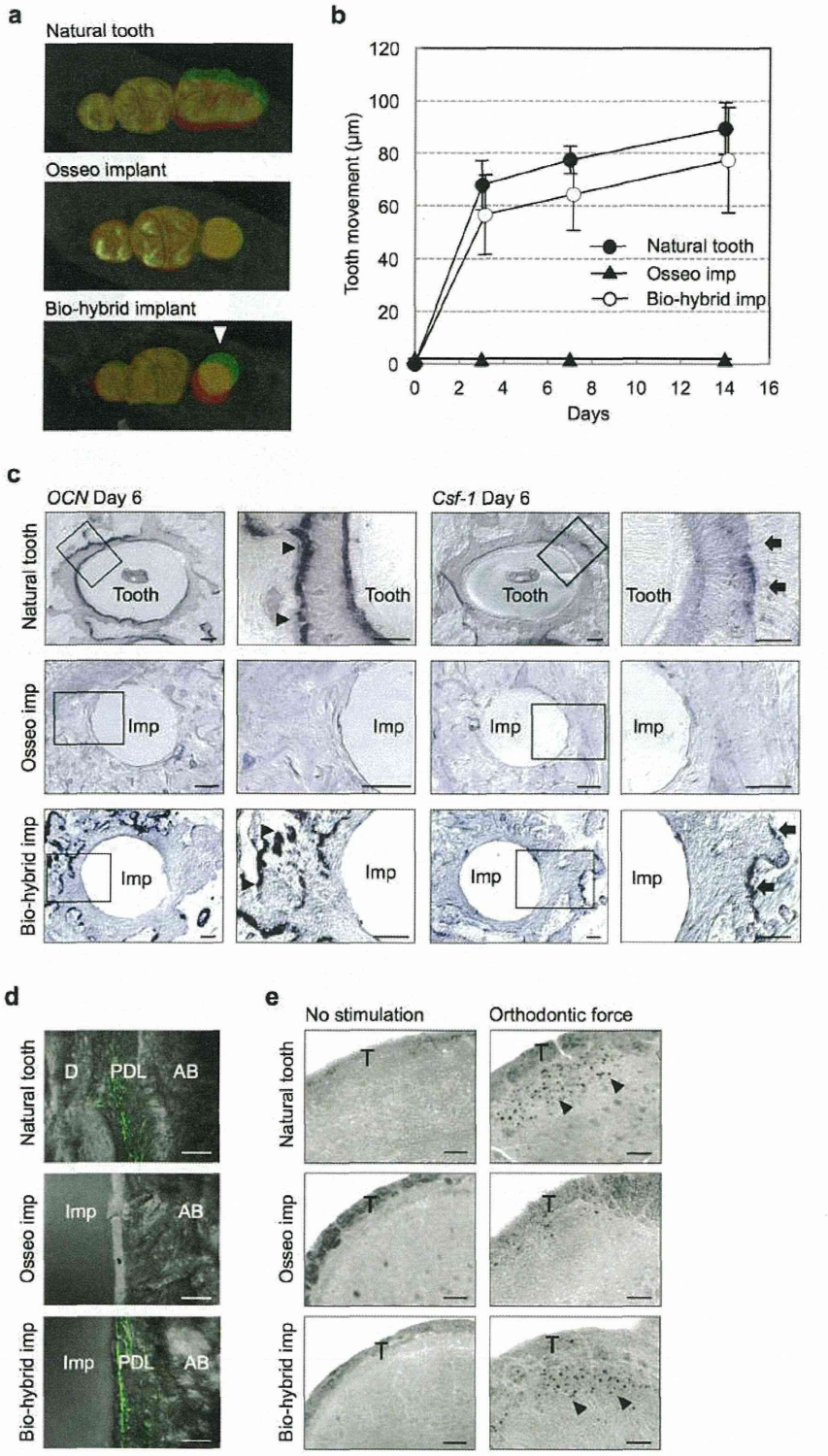

Figure 3 | Functional regeneration of a bio-hybrid implant. (a and b) Horizontal superposition of micro-CT images (*left*) of the natural tooth (*top*), osseo-integrated implant (*middle*) and bio-hybrid implant (*bottom*) at days 0 (red) and 14 days (green) of experimental orthodontic treatment. The movement distances of tooth and both implants by orthodontic force were measured after experimental orthodontic treatment at days 0, 3, 7 and 14 (*right*). Data represent the mean ± s.d.; $n = 5$ for natural tooth, osseo-integrated implant and bio-hybrid implant, respectively. (c) Sections of natural tooth, osseo-integrated and bio-hybrid implants were analysed by *in situ* hybridization analysis for *Ocn* and *Csf-1* mRNA at day 6 of orthodontic treatment. *Ocn* mRNA-positive cells (arrowhead) and *Csf-1* mRNA-positive cells (arrow) are indicated. Scale bar, 100 μm. (d) Nerve fibres in the PDL of the natural tooth (*top*), osseo-integrated implant (*middle*), and bio-hybrid implant (*bottom*) were analysed by immunohistochemistry using specific antibodies for neurofilament (NF; green). Scale bar, 50 μm. D, dentin; AB, alveolar bone; PDL, periodontal ligament; Imp, implant. (e) Analysis of c-Fos immunoreactive neurons in the medullary dorsal horns of mice after 0 hours (no stimulation, control; *left*) and 2 hours of stimulation by orthodontic force (*right*). c-Fos protein (arrowhead) was detectable after stimulation in the natural tooth (*top*) and bio-hybrid implant (*bottom*). Scale bar, 100 μm. T, spinal trigeminal tract.